JOURNAL OF GUIDANCE, CONTROL, AND DYNAMICS
Vol. 22, No. 6, November–December 1999

Active $\mathcal{H}_\infty$ Control of Sound Radiation from Thin Cylindrical Panels

Moshe Idan,* Baruch Pletner,† and Tanchum Weller‡
Technion—Israel Institute of Technology, 32000 Haifa, Israel

Active control of sound radiated by thin-walled cylindrical panels using arrays of spatially discrete piezoelectric sensors and actuators is addressed. A new general methodology for the design of controllers to reduce structure radiated noise is presented. The methodology utilizes finite element modeling to perform structural discretization. The structure dynamics model, presented in state-space form, incorporates simplified models of the piezoelectric sensing and actuation and accounts for the mass and stiffness of the piezoelectric elements. The acoustic power radiated by the structure into the far field is expressed as a quadratic form of the system states that is used to define an acoustic performance criterion in an $\mathcal{H}_\infty$ disturbance rejection controller design setup. The methodology is applied for active control of sound radiated by a vibrating thin cylindrical panel excited by a persistent external force. The controller performance is evaluated using numerical simulations of the controlled structure. It is shown that the sound radiated by the panel into the far field is effectively controlled and reduced.

Introduction

ACTIVE structural acoustic control (ASAC) has been extensively addressed in the literature. In essence, ASAC can be interpreted as attenuation of structure radiated sound resulting from a persistent excitation/disturbance. In controller design terms, it can be viewed as a disturbance rejection problem, the control objective of which is to minimize structure radiated sound, specified by an analytical sound radiation model. This is closely related to conventional vibration suppression control, often obtained by increasing (passively or actively) the damping of the controlled structure, which also reduces the structure radiated sound. Because effective ASAC should tackle the sound radiation mechanisms directly, which, in addition to the vibrational power, includes additional important parameters such as vibrational mode shapes, excitation frequency, and others, use of a controller specifically designed to minimize the sound radiation should be more effective.

As an application of intelligent structures technology, ASAC relies on integrating piezoelectric sensors and actuators, for example, PVDF and PZT, into the structure. Modeling of such an integrated structure has been the subject of on-going research, with initial results reported by Crawley and de Luis,[1] followed by Wang[2] and more recently by Pletner and Abramovich,[3] to name but a few. The sound radiated by a vibrating structure into the far field from measurements of the structural velocity field was investigated, both analytically and experimentally, by Clark and Fuller,[4] Mathur and Tran,[5] and others. The analytical formulation presented in these studies was exclusively performed on simple structures (simply supported beams and plates), while neglecting the mass and stiffness of the sensors and actuators. More complex structures, such as cylindrical shells[6] and airplane fuselage,[7] were treated only experimentally. The ASAC controller designs documented in the literature are limited to proportional and least mean squares algorithms, which are used to control the experimental structure.

To make ASAC applicable for commercial applications, a reliable methodology that covers the design and analysis of adaptive structures with complex geometric and material properties, incorporates a model of the sound radiation mechanism, and includes appropriate control synthesis algorithms is needed. This goal is undertaken in this study, which presents a new methodology that attempts to address ASAC objectives. This methodology, which utilizes finite element (FE) tools to obtain a discrete representation of the continuous structure dynamics of (almost any) linearly elastic thin-walled structural element, incorporating piezoelectric sensing and actuation, uses the recent results of Pletner and Abramovich.[3] Because FE models of continuous structures tend to be very large, making the synthesis, analysis, and implementation of the controlled structure extremely difficult, static condensation and/or balanced truncation[8] techniques are employed to reduce the model dimensions.

The acoustic power radiated by the structure into the far field can be expressed as a quadratic form of the system states. This forms the basis for a controller design setup, where the performance specifications are given by requirements on the allowable acoustic power. The controller synthesis, which includes the sound reduction criteria, sensor noise, and actuation limits, is stated as a disturbance rejection problem in the $\mathcal{H}_\infty$ framework.

The advantage of the methodology proposed herein is in its generality. It is applicable to any linearly elastic structure and permits the application of the latest techniques in state-space multi-input/multi-output control design tools. This study aims at demonstrating the performance and effectiveness of the resulting controller in reducing the sound radiated by a vibrating cylindrical panel.

Methodology Outline

This section summarizes the new proposed methodology, which includes three major parts: the control-oriented modeling of the structural dynamics and piezoelectric actuation and sensing, the derivation of acoustic performance criterion, and the controller design.

Structural Dynamics

Structural response to mechanical or piezoelectric excitation is governed by spatially continuous partial differential equations. Design of model-based controllers requires, however, a finite-dimensional, or spatially discrete, model of the structural dynamics, which in the current methodology is obtained using the FE modeling technique. State-of-the-art FE codes (ANSYS[9] in the present study) allow the analysis of structures with complex boundary conditions and varying elastic and geometric properties. It should be noted that any other method for approximating the structural response by a finite-dimensional system of ordinary differential equations is applicable in conjunction with the controller design methodology discussed in the sequel. The finite-dimensional model of the controlled structure has to account for the mass and stiffness properties of the piezoelectric laminas. Neglecting those may cause noticeable model errors and, consequently, degrade the performance of

Received 3 April 1998; revision received 2 May 1999; accepted for publication 20 May 1999.

*Senior Lecturer, Faculty of Aerospace Engineering. Associate Fellow AIAA.

†Graduate Student, Faculty of Aerospace Engineering; currently Senior Engineer, Active Control Experts (ACX), Inc., Cambridge, MA. Member AIAA.

‡Professor, Faculty of Aerospace Engineering. Associate Fellow AIAA.

the model-based controller. FE modeling provides the mass and stiffness matrices of the structure and the structural load vector. In addition, the frequency and shape of the structural modes, obtained from the FE model, can be used to assess their sound radiation properties and, thus, can guide in placement of the piezoelectric elements. Note that the important issue of optimal actuator and sensor placement was not addressed in this study and is the subject of further research.

The structural load vector included in the FE model consists of the piezoelectric control forces and the external disturbance or excitation forces. (Forces are defined in the generalized sense and include both forces and moments.) In the present FE modeling, the piezoelectric actuation is incorporated by application of the equivalent mechanical loads technique to substitute for the piezoelectric induced strain control inputs.[3] This substitution is of practical importance in using commercial FE codes for modeling of the controlled structure. It provides the flexibility to choose element types that yield maximum accuracy, while retaining a low number of degrees of freedom (DOF) in the finite-dimension representation of the structural dynamics. Note, further, that piezoelectric sensing depends on the type of FEs used in the FE model because modeling of piezoelectric sensing requires incorporation of the structural rotation angles at the edges of the sensors.[10]

To comply with the format of many modern model-based controller design techniques, the finite-dimensional structural dynamics model obtained using FE is presented in state-space form. The input matrix is constructed using the electrical-to-mechanical scaling coefficients found utilizing the tools of Ref. 3, whereas the measurements matrix is constructed using the model of piezoelectric sensing.[11]

FE models of complex structures may contain thousands of DOF, resulting in very large dynamics models. Controllers for systems of this order cannot be synthesized by the currently available numerical design tools. Hence, it is necessary to reduce the order of the system, without significantly degrading model accuracy. In the current design methodology this is done in two stages: First, a reduced FE model is obtained using the static condensation technique[12]; second, following the construction of the state-space model and the formulation of the performance criterion, balanced truncation is used to reduce the system order even further.[8]

Acoustic Performance Criteria

The total acoustic power radiated by a thin-walled vibrating structures into the far field[13] is used as the main controller performance criterion in this study. Utilizing the wave number theory, the acoustic power is derived as a function of the structural velocity field, presented in the spatially continuous (infinite-dimensional) form. These analytical expressions are discretized and expressed as a quadratic function of the finite-dimensional system states. The approximate quadratic expressions of the acoustic power are defined as ASAC performance criterion. Together with the finite-dimensional model of the structure dynamics, this criterion is suitable for many modern controller synthesis schemes, for example, linear quadratic Gaussian, $\mathcal{H}_\infty$, μ, etc.

Controller Design

It is assumed that the structure radiated sound results from steady-state vibrations excited by a persistent, narrowband and power-bounded external force and that the controlled structure is closed-loop stable and, thus, does not generate energy. This ensures that the structural outputs, which consist of mechanical vibrations and sound radiation, are also persistent power-bounded processes. Rejection of power-bounded response due to power-bounded input can be naturally cast as an $\mathcal{H}_\infty$ disturbance rejection control problem.[14] Other suitable controller design techniques may also be used with the general state-space formulation of the structural dynamics and the aforementioned quadratic performance criterion.

In addition to the main acoustic performance criterion, the $\mathcal{H}_\infty$ controller synthesis procedure can incorporate limits on the maximum driving voltage inputs to the piezoelectric actuators, dynamics characteristics (bandwidth, scaling, and range) of the piezoelectric sensors, their measurement noise characteristics, and more. The characteristics of the piezoelectric elements can be obtained from manufacturers data sheets or from experiments. Additional noise signals and uncertainty blocks can be introduced in the controller synthesis setup as design parameters to compensate for the modeling inaccuracies due to model order reduction, model parameter uncertainties, and more.

Design Methodology: Summary

The present design methodology, which covers the modeling, acoustics, and controller design aspects of ASAC, is discussed in detail in Ref. 11. For completeness, a brief outline of each step of this methodology is presented in the following sections, followed by a detail ASAC design for a thin-walled cylindrical panel.

Structural Dynamics with Piezoelectric Sensing and Actuation

Using a curvilinear coordinate system $(\alpha_1, \alpha_2, \alpha_3)$ for modeling thin panels, it is assumed that their dimensions in one direction (α_3) are much smaller than those in the (α_1, α_2) directions. During vibrations, the transverse α_3 component of the resulting structural velocity affects the surrounding fluid medium and can radiate sound into the far field. Therefore, active control of this sound radiation requires control of the transverse velocities.

The FE method is applied to obtain a discretized model of the structure dynamics. This model also incorporates the piezoelectric actuation and sensing. The general form of such a model, excited by N_e external forces $f^i(t)$, and controlled by N_a voltage inputs $V_a^j(t)$ to the piezoceramic actuators, is represented by

$$\boldsymbol{M}\ddot{\boldsymbol{d}} + \boldsymbol{C}_d\dot{\boldsymbol{d}} + \boldsymbol{K}\boldsymbol{d} = \sum_{i=1}^{N_e} \boldsymbol{F}_e^i f^i(t) + \sum_{j=1}^{N_a} \boldsymbol{F}_a^j V_a^j(t) \tag{1}$$

where $\boldsymbol{M}, \boldsymbol{C}_d$, and $\boldsymbol{K}$ are the global mass, damping, and stiffness matrices, respectively; $\boldsymbol{d}$ is the nodal displacement vector, $\boldsymbol{F}_e^i$ is the load coefficient vector generated by the FE model for the ith external excitation force, and $\boldsymbol{F}_a^j$ is the load coefficient vector for the jth actuator. Equation (1) was obtained after static condensation, that is after eliminating some of the FE DOF without noticeably affecting the low-frequency behavior of the model.

The model of Eq. (1) is easily transformed into the state-space form

$$\dot{\boldsymbol{x}} = \boldsymbol{A}\boldsymbol{x} + \boldsymbol{B}\begin{Bmatrix} \boldsymbol{f} \\ \boldsymbol{V}_a \end{Bmatrix}, \qquad \boldsymbol{x} \triangleq \begin{Bmatrix} \boldsymbol{d} \\ \dot{\boldsymbol{d}} \end{Bmatrix} \tag{2}$$

$$\boldsymbol{y} = \boldsymbol{C}_y\boldsymbol{x} \tag{3}$$

$$\boldsymbol{v} = \boldsymbol{C}_v\boldsymbol{x} \tag{4}$$

where $\boldsymbol{y}$ is the vector of the piezoelectric measurements and $\boldsymbol{v}$ is the nodal velocity vector that is used to calculate the far-field acoustic power in the next section. The vectors $\boldsymbol{f}$ and $\boldsymbol{V}_a$ contain the excitation forces and control voltages, respectively.

The voltage measured across a piezoelectric sensor is a function of the transverse motion $w(\alpha_1, \alpha_2)$ of the structure. For thin-walled structures this motion can be approximately expressed as a product of two single-coordinate functions

$$w(\alpha_1, \alpha_2) = w_1(\alpha_1)w_2(\alpha_2)$$

As shown by Pletner and Abramovich,[10] the voltage measured across a single layer piezoelectric sensor (the lth sensor) that constitutes a generalized rectangle in the (α_1, α_2) plane is given by

$$\tilde{V}_l = -\frac{he_{31}^l}{C_l}\int_{\alpha_1^{l,L}}^{\alpha_1^{l,R}} w_1''(\alpha_1)\,\mathrm{d}\alpha_1 - \frac{he_{32}^l}{C_l}\int_{\alpha_2^{l,B}}^{\alpha_2^{l,F}} w_2''(\alpha_2)\,\mathrm{d}\alpha_2$$

$$= -\frac{he_{31}^l}{C_l}\left[w_1'\left(\alpha_1^{l,R}\right) - w_1'\left(\alpha_1^{l,L}\right)\right] - \frac{he_{32}^l}{C_l}\left[w_2'\left(\alpha_2^{l,F}\right) - w_2'\left(\alpha_2^{l,B}\right)\right] \tag{5}$$

where h is half the plate thickness, e_{31}^l and e_{32}^l are the piezoelectric constitutive parameters, and C_l is the sensor capacitance. Here, $\alpha_1^{l,L}$, $\alpha_1^{l,R}$, $\alpha_2^{l,B}$, and $\alpha_2^{l,F}$ are the left, right, back, and front edge coordinates of the sensor.

The continuous presentation of the piezoelectric sensing given in Eq. (5) can be approximated using the spatially discretized model of the structural dynamics, Eqs. (2) and (3), through the elements of the matrix $\boldsymbol{C}_y$. The actual expressions depend on the type of the FEs used in the modeling. For elements that include rotational DOF, such as the ANSYS SHELL elements,[9] the slopes in Eq. (5) are a subset of the model DOF and, thus, of the state space vector. In this case $\boldsymbol{C}_y$ will be constructed of the terms $\pm he_{31}^l/C_l$ and $\pm he_{32}^l/C_l$ in the appropriate locations, determined by the sensor location and geometry. If only translational DOF constitute the structural dynamics model, for example, using only ANSYS SOLID elements,[9] these slopes can be approximated using finite differences between adjacent node translations[11]

$$w_1'\left(\alpha_1^{l,R}\right) \cong \frac{w_{\alpha_1^{l,R+1}} - w_{\alpha_1^{l,R-1}}}{\Delta\alpha_1} \tag{6}$$

where, $w_{\alpha_1^{l,R+1}}$ and $w_{\alpha_1^{l,R-1}}$ are the displacements of the nodes adjacent to the edge node $\alpha_1^{l,R}$ and $\Delta\alpha_1 = \alpha_1^{l,R+1} - \alpha_1^{l,R-1}$. Because these displacements are part of the state vector $\boldsymbol{x}$, the appropriate elements of $\boldsymbol{C}_y$ will be $\pm he_{31}^l/(C_l\Delta\alpha_1)$ and $\pm he_{32}^l/(C_l\Delta\alpha_2)$.

The matrix $\boldsymbol{C}_v$ is constructed as

$$\boldsymbol{C}_v = [\boldsymbol{0} \mid \hat{\boldsymbol{C}}] \tag{7}$$

where the elements of $\hat{\boldsymbol{C}}$ are set to 1 at the locations of the transversal nodal velocities that are a subset of the velocity vector $\boldsymbol{d}$.

Sound Radiation from Thin-Walled Structures

The theory of sound radiation by structural vibration presented in this section assumes that only the transverse component of the structural velocity field can radiate sound and that the structural displacements are small. This theory assumes that sound radiated by structural vibration is different in the low- and high-frequency ranges. The particular frequency separating these two bands is called the cutoff or critical frequency ω_c (Ref. 13). At this frequency, the structural and acoustic wavelengths coincide, which is expressed as

$$\omega_c = c^2\sqrt{\bar{\rho}/D} \tag{8}$$

where c is the speed of sound in the surrounding fluid medium, $\bar{\rho}$ is the structure mass per unit area, and D the bending stiffness of the structure.[13]

The radiation efficiency σ of the structure is defined as the ratio of the total normalized acoustic power radiated into the far field to the spatial and temporal average of the squared structural velocity field $\langle v^2(\alpha_1, \alpha_2, t)\rangle$. When the structural response is expressed as a modal sum, the (m, n) modal radiation efficiency of a generalized rectangular structure in the (α_1, α_2) plane takes on the form

$$\sigma_{mn} = \frac{P/\rho c L_1 L_2}{\left\langle v_{mn}^2(\alpha_1, \alpha_2, t)\right\rangle} \tag{9}$$

where P is the acoustic power, ρ is the structure density, and L_1 and L_2 are the structure's dimensions in (α_1, α_2) coordinates. The index pair (m, n) denotes the structural mode number or the number of bending half-waves in the (α_1, α_2) directions. For frequencies higher than ω_c, the sound intensity radiated by the vibrating structure is largely independent of the modal order and, therefore, of the vibrational shape.[15] In the $\omega < \omega_c$ frequency range, the radiation efficiency varies widely with the modal order, that is, the spatial distribution of the structural velocity field.

As is apparent from Eq. (8), the critical frequency is directly proportional to the square root of the structural mass density to stiffness ratio. Hence, heavy, compliant structures will have a higher critical frequency than light, stiff ones. Note that, although in general the radiation efficiency at frequencies below the critical are relatively low, there can be low-frequency structural modes that efficiently radiate sound into the surrounding medium. Furthermore, the frequency spectrum of up to 5 kHz, typical of cutoff frequencies for thin plates, is particularly unpleasant and even damaging to humans.[16]

Passive sound attenuation, obtained by attaching a layer of low stiffness-to-mass ratio material to the vibrating structure, however, increases ω_c and structural damping. This could be undesirable, especially in lightweight structures (like airframes). Furthermore, this yields a large frequency band $\omega < \omega_c$ for which the sound radiation efficiency is generally lower, but displays a strong dependence on the modal order and subsequently on the vibrational shape of the structure. Therefore, the attenuation of the radiated sound below the critical frequency has to be treated by active sound control schemes. Thus, a combination of passive and active sound control techniques will provide the best available solution to the problem of the reduction of structure radiated sound over a broad frequency range.

Efficient active acoustic control requires a reliable model of the sound radiation mechanism. In addition, it is important that this model can be incorporated within an appropriate controller design methodology framework. The well-established wave number theory for structure sound radiation is used here to develop an acoustic performance criterion that utilizes the discretized model of the structural dynamics. In particular, in the case of steady-state sound radiation due to a single frequency excitation, a quadratic performance criterion is obtained. This criterion is suitable for a multitude of controller synthesis and analysis methods and, thus, was adopted in the current study.

Note that the wave number theory is applicable to the current analysis only if the following two assumptions are met: nonlinear structural behavior, regardless of its origin, may be neglected and any discontinuities in the structural elements, such as holes, stiffeners, etc., do not significantly affect the bending wave propagation mechanism. In the case of significant nonlinearities and structural discontinuities, the structural elements may be redefined, or a numerical approach may be adopted in lieu of the current analysis.

Continuous Formulation

The steady-state response of a thin-walled structure excited by a single frequency force is given by

$$v(\alpha_1, \alpha_2, t) = V(\alpha_1, \alpha_2)e^{J\omega t} \tag{10}$$

where $V(\alpha_1, \alpha_2)$ is the steady-state spatial vibrational shape and ω is the excitation frequency. The total acoustic power radiated by the structure into the far field is given by[13]

$$P = \frac{\omega\rho}{8\pi^2}\iint_{A_r} \frac{|\hat{v}(k_1, k_2)|^2}{\sqrt{k_a^2 - k_1^2 - k_2^2}}\,\mathrm{d}k_1\,\mathrm{d}k_2 \tag{11}$$

where $k_a \triangleq \omega/c$ is the acoustic wave number and k_1 and k_2 are the structural wave numbers; the integration is performed over the radiating circle A_R, defined by $k_1^2 + k_2^2 = k_a^2$, and the transformed velocity field $\hat{v}(k_1, k_2)$ is defined by

$$\hat{v}(k_1, k_2) = \iint_A V(\alpha_1, \alpha_2)\exp[J(k_1\alpha_1 + k_2\alpha_2)]\,\mathrm{d}A \tag{12}$$

where A is the total area of the structure.

The sound intensity L_W, sometimes referred as sound pressure level (SPL), can be expressed in the familiar decibel units as[16]

$$L_W = 10\log_{10}(P/P_0) \tag{13}$$

where $P_0 = 1 \times 10^{-12}$ W/m^2 is the sensitivity threshold of the human ear for standard atmospheric conditions at sea level.

State-Space Formulation

Because of the complex form of Eqs. (11) and (12), analytical evaluation of the acoustic power for general boundary conditions is impossible.[13] Therefore, a discrete approximation of the acoustic power is derived for the discretized FE model of the structure dynamics.

The steady-state structural response for a single frequency excitation is expressed as

$$\boldsymbol{v}_{ss}(t) = \boldsymbol{C}_v \boldsymbol{x}_{ss}(t) = \boldsymbol{C}_v \boldsymbol{X} e^{J\omega t} \triangleq \boldsymbol{V} e^{J\omega t} \tag{14}$$

where $\boldsymbol{X}$ and $\boldsymbol{V}$ are the steady-state displacement and velocity shapes, respectively. To approximate the acoustic power, the spatial and the wave number domains must be discretized. The spatial domain (in the in-plane directions) was already discretized by the FE model, leading to a spatial mesh with $N = N_1 \times N_2$ elements, where N_1 and N_2 are the number of elements in the (α_1, α_2) directions, respectively. Next, the two-dimensional structural wave number domain is discretized as

$$\boldsymbol{k}_1 = \begin{bmatrix} k_1^1 & \cdots & k_1^r & \cdots & k_1^{N_k^1} \end{bmatrix}^T$$

$$\boldsymbol{k}_2 = \begin{bmatrix} k_2^1 & \cdots & k_2^q & \cdots & k_2^{N_k^2} \end{bmatrix}^T$$

An approximate expression for the transformed velocity field is obtained by evaluating Eq. (12) at discrete (k_1^r, k_2^q) and numerically integrating it over the discretized spatial domain

$$\hat{v}\left(k_1^r, k_2^q\right) \approx \sum_{m=1}^{N} V_m \exp\left[J\left(k_1^r \alpha_1^m + k_2^q \alpha_2^m\right)\right] \delta A_m \triangleq \boldsymbol{\Theta}_{rq} \boldsymbol{V} \tag{15}$$

where V_m and δA_m are the velocity and the area of the mth element, respectively, and $\boldsymbol{\Theta}_{rq}$ is a complex row vector. Using Eq. (15), the square modulus of the transformed discrete velocity can be expressed in a compact quadratic matrix form

$$\left|\hat{v}\left(k_1^r, k_2^q\right)\right|^2 = \boldsymbol{V}^T \boldsymbol{\Theta}_{rq}^* \boldsymbol{\Theta}_{rq} \boldsymbol{V} \triangleq \boldsymbol{V}^T \boldsymbol{Q}_{rq} \boldsymbol{V} \tag{16}$$

where $(\,)^*$ denotes a complex conjugate transpose. In the quadratic form of Eq. (16), only the symmetric part of $\boldsymbol{Q}_{rq}$ can be retained. Because $\boldsymbol{Q}_{rq} = \boldsymbol{\Theta}_{rq}^* \boldsymbol{\Theta}_{rq}$, it is a standard result that the imaginary part of $\boldsymbol{Q}_{rq}$ is antisymmetric, and, therefore, Eq. (16) can be written as

$$\left|\hat{v}\left(k_1^r, k_2^q\right)\right|^2 = \boldsymbol{V}^T \Re(\boldsymbol{Q}_{rq}) \boldsymbol{V} \tag{17}$$

where $\Re(\,)$ is the real part of $(\,)$.

Using the discrete wave number field, the acoustic power [Eq. (11)] is approximated

$$P \approx \bar{\omega} \sum_{r=1}^{N_k^1 - 1} \sum_{q=1}^{N_k^2 - 1} \left[\frac{\left|\hat{v}\left(k_1^r, k_2^q\right)\right|^2}{\sqrt{k_a^2 - \left(k_1^r\right)^2 - \left(k_2^q\right)^2}} \delta k_1^r \delta k_2^q \right]$$

$$= \bar{\omega} \sum_{r=1}^{N_k^1 - 1} \sum_{q=1}^{N_k^2 - 1} \beta_{rq} \left|\hat{v}\left(k_1^r, k_2^q\right)\right|^2 \tag{18}$$

where

$$\bar{\omega} \triangleq \frac{\omega \rho}{8\pi^2}, \qquad \delta k_{1,2}^{r,q} \triangleq k_{1,2}^{r+1,q+1} - k_{1,2}^{r,q}$$

$$\beta_{rq} \triangleq \frac{\delta k_1^r \delta k_2^q}{\sqrt{k_a^2 - \left(k_1^r\right)^2 - \left(k_2^q\right)^2}}$$

Introducing Eq. (17) into Eq. (18) yields

$$P = \bar{\omega} \sum_{r=1}^{N_k^1 - 1} \sum_{q=1}^{N_k^2 - 1} \boldsymbol{V}^T [\beta_{rq} \Re(\boldsymbol{Q}_{rq})] \boldsymbol{V} = \boldsymbol{V}^T \boldsymbol{Q}_v \boldsymbol{V} \tag{19}$$

where

$$\boldsymbol{Q}_v = \bar{\omega} \sum_{r=1}^{N_k^1 - 1} \sum_{q=1}^{N_k^2 - 1} \beta_{rq} \Re(\boldsymbol{Q}_{rq}) \tag{20}$$

To express the acoustic power in terms of the time-dependent system states, the following algebraic manipulation, valid for all T, is performed:

$$P = \boldsymbol{V}^T \boldsymbol{Q}_v \boldsymbol{V} = \boldsymbol{V}^T \boldsymbol{Q}_v \boldsymbol{V} \left[\frac{1}{T} \int_0^T (e^{-J\omega t} e^{J\omega t})\, \mathrm{d}t \right]$$

$$= \frac{1}{T} \int_0^T (\boldsymbol{V} e^{J\omega t})^* \boldsymbol{Q}_v (\boldsymbol{V} e^{J\omega t})\, \mathrm{d}t \tag{21}$$

and using Eq. (14) leads to

$$P = \frac{1}{T} \int_0^T \boldsymbol{x}_{ss}^*(t) \boldsymbol{C}_v^T \boldsymbol{Q}_v \boldsymbol{C}_v \boldsymbol{x}_{ss}(t)\, \mathrm{d}t \tag{22}$$

Motivated by this equation, the transient stage acoustic power is approximated by the following time average:

$$\bar{P} = \frac{1}{T} \int_0^T \boldsymbol{x}^*(t)^T \boldsymbol{C}_v^T \boldsymbol{Q}_v \boldsymbol{C}_v \boldsymbol{x}(t)\, \mathrm{d}t \tag{23}$$

It is obvious that in steady state $P = \bar{P}$.

The symmetric matrix $\boldsymbol{Q}_v$, defined in Eq. (20) as a weighted sum of the matrices $\Re(\boldsymbol{Q}_{rq})$, can be decomposed as

$$\boldsymbol{Q}_v = \bar{\boldsymbol{Q}}_v^T \bar{\boldsymbol{Q}}_v \tag{24}$$

From Eq. (16), we can deduce that $\operatorname{rank}\{\Re(\boldsymbol{Q}_{rq})\} \leq 2$, and therefore, $\operatorname{rank}\{\boldsymbol{Q}_v\} \triangleq r \leq N$. Consequently, $\bar{\boldsymbol{Q}}_v$ is a full row rank matrix of dimension $r \times N$.

Using these results in Eq. (23) and scaling it by the sensitivity threshold P_0 Eq. (13), we obtain

$$P_{\text{scaled}} = \frac{1}{T} \int_0^T \left[\boldsymbol{x}^T(t) \boldsymbol{C}_a^T\right] [\boldsymbol{C}_a \boldsymbol{x}(t)]\, \mathrm{d}t \triangleq \frac{1}{T} \int_0^T \boldsymbol{p}^T(t) \boldsymbol{p}(t)\, \mathrm{d}t \tag{25}$$

where

$$\boldsymbol{C}_a \triangleq \left(1/\sqrt{P_0}\right) \bar{\boldsymbol{Q}}_v \boldsymbol{C}_v \tag{26}$$

and

$$\boldsymbol{p}(t) = \boldsymbol{C}_a \boldsymbol{x}(t), \qquad \dim[\boldsymbol{p}(t)] = r \tag{27}$$

The SPL is expressed as

$$L_W = 10 \log_{10} P_{\text{scaled}} \tag{28}$$

Equations (25–27) approximate the steady-state acoustic power radiated by the structure into the far field using the time-dependent system states. These expressions can now be incorporated into the controller design procedure for explicit active attenuation of structure radiated sound, as is presented next.

Balanced Model Reduction

Dimensions of state-space representations of the structural dynamics, as obtained by FE modeling, tend to be very large. In the ASAC context, the large number of DOF is required for accurate representation of the spatial velocity field, used to obtain a reliable approximation of the structure radiated acoustic power. However, because of the relatively small number of actuators and sensors used in actual implementations, some of the discretized system modes will be only lightly controllable and/or observable. This could increase the computational complexity and cause numerical difficulties in controller synthesis. To comply with computational efficiency requirements and practical implementation considerations, systems models with a relatively small number of states are desirable for control synthesis.

Low-order systems can be efficiently obtained using the balanced model reduction technique.[8] This may lead to a substantial reduction in the number of states. For the truncation, the outputs of the structure dynamics model include both the piezoelectric measurements given by Eq. (3) and the variable $\boldsymbol{p}(t)$ of Eq. (27) used to compute the acoustic power. Proper location of the actuators and sensors is crucial

for efficient ASAC and affects the balanced truncation process. In general, actuators and sensors should be placed in areas of expected maximal structural bending moments. The optimal placement and sizing of the piezoelectric elements was not covered in the current study and is the subject of ongoing research, in which the balanced realization technique could serve as a central synthesis and analysis tool.

$\mathcal{H}_\infty$ ASAC Design Setup

ASAC can be formulated as a disturbance rejection control problem[14] and can be solved by using readily available software.[17] The structure is excited by a persistent external force or by an acoustic pressure, interpreted as disturbances to the system. The goal is to attenuate the far-field steady-state structure radiated acoustic power. The results presented here assume that the structure dynamics model is known exactly (no model uncertainty). Model errors that may result from modeling simplifications or the model reduction and truncation procedures discussed earlier can be also incorporated in this controller synthesis scheme.

The $\mathcal{H}_\infty$ ASAC design setup is shown schematically in Fig. 1. This setup incorporates the model of the structural dynamics (given by the FE discretization), piezoceramic actuator dynamics, and various frequency weighting functions that specify the controlled system performance requirements and limitations. Additional blocks can be added to the model of Fig. 1 to represent system uncertainties. All of the inputs and outputs in this interconnection model can be vector variables, depending on the particular ASAC setup. In this setup, the external inputs consist of the scaled mechanical or acoustic surface loads $\tilde{f}$ and the scaled measurement noises $\tilde{n}$. The generalized outputs include the scaled system variables $\tilde{p}$ used to express the acoustic power radiated by the structure into the far field and the scaled controller commands $\tilde{u}$.

The performance weighting function W_e specifies the acoustic power reduction requirements of ASAC and is set to $1/\sqrt{(P_{\max})} \cdot I_{r\times r}$, where $r = \dim(\boldsymbol{p})$ and $P_{\max}$ is the maximum allowable acoustic power computed by Eq. (25). The band-limited external force f is modeled by the weighting function $W_d(s)$, shaped as a bandpass filter at the corresponding frequency and a peak gain that corresponds to the load magnitude F_a. This approximates a single frequency excitation $f(t) = F_a e^{j\omega_a t}$ that can be handled by the acoustic radiation model adopted in this study.

Piezoceramic actuators dynamic response is usually represented by a high-pass filter, because they have a very limited direct current capability. In this study, however, no dc or low-frequency actuation is required, and all of the performance requirements are limited to frequencies well within the actuators operation range. Therefore, the actuators dynamics are neglected and the W_a block could be omitted or set to $W_a = I_{N_a\times N_a}$. The voltage input to the piezoceramic actuators is limited by the maximum allowable driving voltage, which may decrease with frequency. In some cases this voltage is limited by the available power source and not by the actuators themselves. The controller design setup of Fig. 1 accounts for these limits by the weighting function W_u that is set to $1/V_{\max} \cdot I_{N_a\times N_a}$, where $V_{\max}$ is the maximum allowable driving voltage. The measurement noise of the piezoelectric sensors is assumed to be a zero mean, white Gaussian stochastic process with standard deviation σ_{N_s}, modeled by $W_n = \sigma_{N_s} \cdot I_{N_s\times N_s}$.

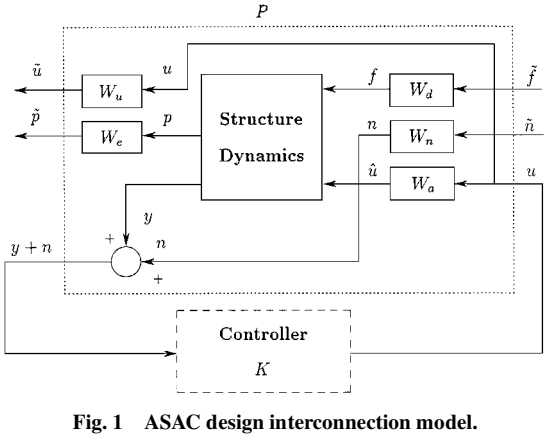

Fig. 1 ASAC design interconnection model.

ASAC of a Thin Cylindrical Panel

In this section an active controller is designed to attenuate the sound radiated by a shallow cylindrical panel at its first two vibrational modes. For thin curved flexible panels it is common to have closely spread natural frequencies corresponding to vastly different modal shapes, as is the case for the second and third modes in this example. Hence, the performance of the second mode controller is examined for third mode excitation. The evaluation also includes a comparison between controllers designed using the acoustic criterion presented earlier and controllers designed for reducing the vibrational power. The latter are synthesized using the interconnection model of Fig. 1 while replacing $\boldsymbol{p}$ with $\boldsymbol{v}$ as the performance outputs.

Geometry and Modeling

ASAC of a shallow aluminum cylindrical panel clamped along its curved edges and simply supported along its long straight edges is investigated. The panel radius of curvature is 1 m. The panel is 0.001 m thick and 0.6 m long, and it spans an arc of 15 deg. These dimensions are representative of fuselage panels in mid-size commercial jets. The panel was modeled using 100 ANSYS SHELL93 eight-node elastic shell elements,[9] which was found to represent the structural dynamics with sufficient accuracy. This resulted in 1563 DOF, which were reduced to 117 by static condensation. The FE model of the panel is shown in Fig. 2, where the grey areas represent the piezoelectric elements. The panel is made of aluminum with $E_{11} = 70$ GPa, Poisson's ratio $\nu_{12} = 0.3$, and mass density $\rho = 2400$ kg/m^3. The PZT and PVDF material properties are: $E_{11}^{\mathrm{PZT}} = 58$ GPa, $\nu_{12}^{\mathrm{PZT}} = 0.3$, and $\rho^{\mathrm{PZT}} = 7800$ kg/m^3; $E_{11}^{\mathrm{PVDF}} = 2$ GPa, $\nu_{12}^{\mathrm{PVDF}} = 0.3$, and $\rho^{\mathrm{PVDF}} = 1780$ kg/m^3. Their piezoelectric properties are: strain constants $d_{31}^{\mathrm{PZT}} = 180 \times 10^{-12}$ m/V and $d_{31}^{\mathrm{PVDF}} = 23 \times 10^{-12}$ m/V, strain ratio $d_{32}^{\mathrm{PZT}} = 180 \times 10^{-12}$ m/V and $d_{31}^{\mathrm{PVDF}} = 3 \times 10^{-12}$ m/V, and capacitance modulus of 379×10^{-8} F/m^2 for both PZT and PVDF.

Preliminary Acoustic Analysis

To determine the structural modes that radiate sound into the surrounding medium, the open-loop acoustic radiation efficiency, given by Eq. (9), was determined for the first three modes: $\sigma_{12} = 0.14$, $\sigma_{13} = 0.90$, and $\sigma_{22} = 0.05$. Clearly, the second mode radiates sound most efficiently, whereas the efficiencies of the first and third modes are lower by factors of about 8 and 20, respectively. The mechanism behind these results is better understood by examining Figs. 3–5, which show the spatial and transformed velocity distributions for the first two fundamental vibrational modes. The higher transformed velocity distribution of the second mode indicates the higher acoustic power of that mode [see Eq. (11)].

Because of the extremely low radiation efficiency of the third mode, controllers for the first and second modes only were synthesized. Because of the similarity in the first and second mode shapes,

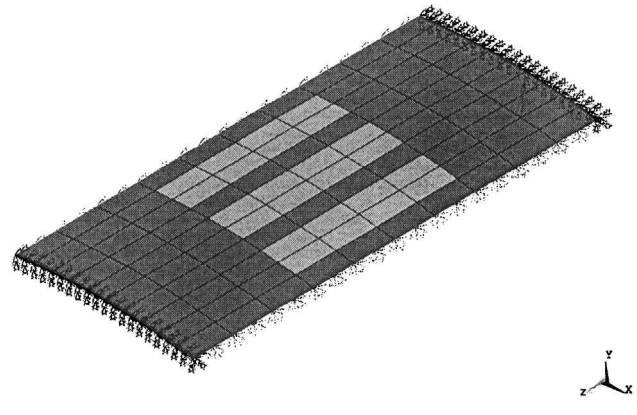

Fig. 2 FE model of a controlled shallow cylindrical shell; gray areas are the piezoelectric elements.

Table 1 Effect of the piezoelectric elements on the first three natural frequencies of the cylindrical panel, Hz

Model	1st mode	2nd mode	3rd mode
No PZT, full model	237.4	336.3	377.7
PZT, full model	216.0	344.9	362.8
PZT, reduced model	216.0	345.2	363.5

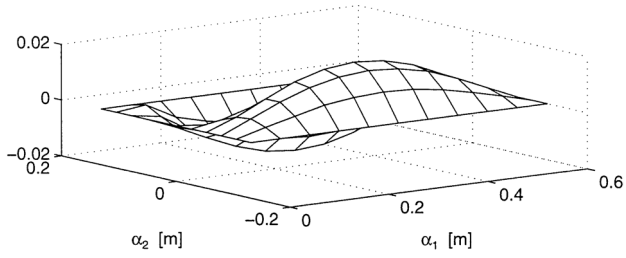

Spatial velocity distribution

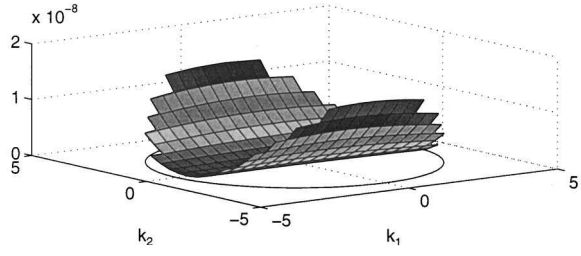

Transformed velocity distribution

Fig. 3 First mode open-loop spatial and transformed velocity distributions.

the piezoelectric sensors and actuators were sized and placed to cover the areas of highest strain of the second mode vibrational shape (see Fig. 2). This arrangement of sensors and actuators proved effective for controlling the sound radiation of these two modes.

Next, the effect of the mass and stiffness of the piezoelectric elements on the overall system dynamics was evaluated using FE models with and without these elements. The natural frequencies of the first three modes were compared for three models: cylindrical panel only, the panel with the piezoelectric elements, and the latter after static condensation. The results are presented in Table 1. The considerable variation in the frequency values obtained for models that include the mass and stiffness of the piezoelectric elements clearly indicates the necessity of these inclusions. The small effect of the order reduction on the model accuracy verified its validity for the controller synthesis.

Controller Design

Following the placement of the piezoelectric elements, balanced model truncation was performed to reduce the order of the system model, while including the various performance specification variables ($\boldsymbol{p}$ or $\boldsymbol{v}$) as additional outputs. In both cases, the order of the system was reduced from 234 to 85 states. Full-order 85 state controllers were implemented in the subsequent analyses, without performing additional controller order reduction. A total of four $\mathcal{H}_\infty$ controllers were constructed.

In the design, the maximum voltage commands to the piezoelectric actuators was set to a realistic value of $V_{\max} = 100$ V, and the measurements noise standard deviation was selected as $\sigma_{N_s} = 0.01$ V. The bandpass frequency of the excitation shaping filter W_d was adjusted according to the first and second mode frequencies of the structure. The maximum allowable acoustic power $P_{\max}$ for the acoustic controllers synthesis and the maximum vibrational power for the vibration controllers design were determined iteratively to obtain maximum attenuation.

Simulation and Discussion

The full-order model of the controlled structure was simulated using the various controllers and external force excitation frequencies.

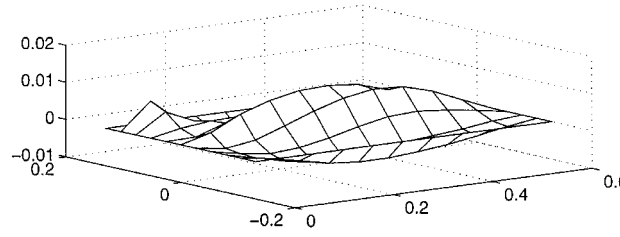

Open loop

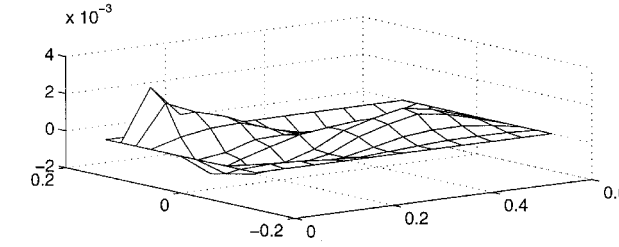

Vibration control

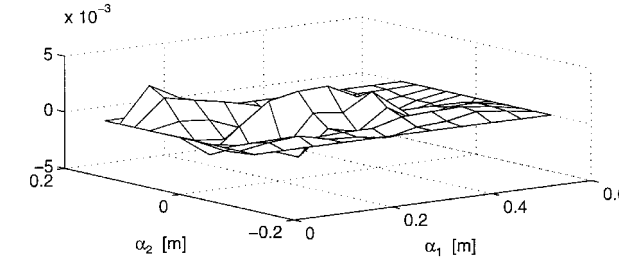

ASAC

Fig. 4 Open- and closed-loop spatial and velocity distributions: second mode control.

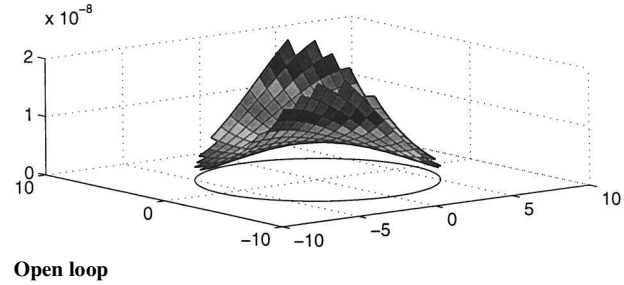

Open loop

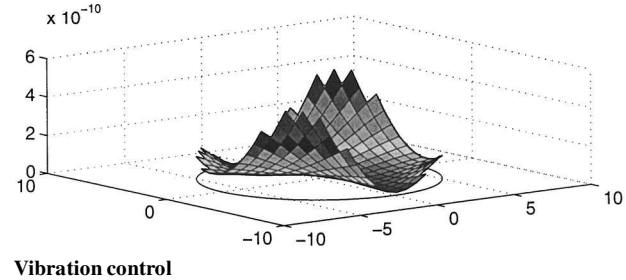

Vibration control

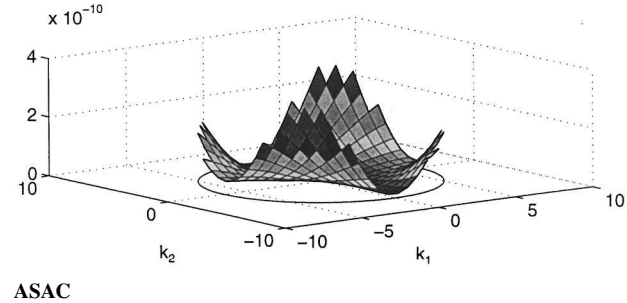

ASAC

Fig. 5 Open- and closed-loop transformed velocity distributions: second mode control.

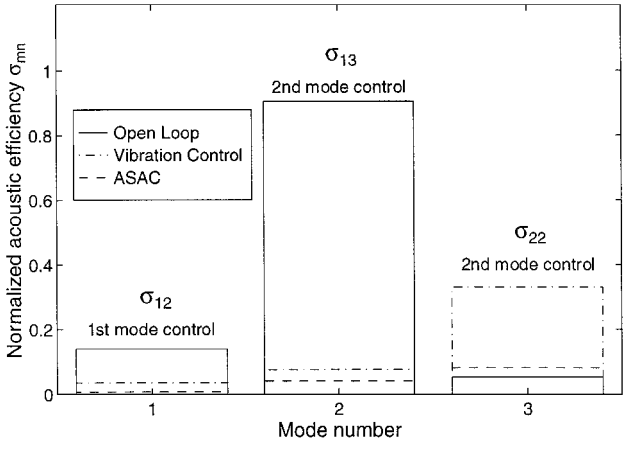

Fig. 6 Open- and closed-loop radiation efficiencies for the first three modes.

In this manner the model reduction effects could be evaluated quantitatively. In addition, second mode controller performance was examined for the closely located third mode excitation, which partially evaluates the robustness properties of the controller.

The overall performance of the acoustic and vibration controllers are examined by the open- and closed-loop radiation efficiencies of the first three vibrational modes, shown in Fig. 6. The first and second mode frequency excitation cases were simulated with acoustic and vibration controllers designed specifically for these frequencies. It is evident that both the acoustic and the vibration controllers proved very effective in reducing the radiation efficiency of these modes, with a clear advantage of the acoustic control.

A larger difference between the acoustic and the vibration control can be observed in the effect of the second mode control on the radiation efficiency of the third mode, which is open loop nonradiating. The second mode acoustic controller caused only a minor increase in the closed-loop radiation efficiency of the third mode, thus, proving itself to be (at least partially) robust to a certain level of fluctuation in the excitation frequency. The second mode vibration controller, however, increased the radiation efficiency of the third mode almost seven times of its open-loop value, making it an even more efficient sound radiator than the first mode in open loop and the second mode in closed-loop. This result shows that vibration controllers can potentially increase the radiation efficiency of open-loop poorly radiating modes. The implication is that low radiation efficiency modes, which may have been neglected or truncated in model reduction, can potentially become closed-loop radiating due to vibration controller spilloverlike effects. This undesirable phenomenon may be reduced by using the ASAC design methodology, as is clearly demonstrated in this study.

The SPL reductions achieved by the first and second mode controllers are presented in Table 2. Clearly, both the acoustic and vibration controllers were able to achieve significant reductions in the sound radiated by the first two vibrational modes. These reductions ranged from 28 to 48% of the uncontrolled SPL. ASAC performed better than vibration control by a margin of 6–7%.

Further insight into the controllers performance is gained from the examination of open- and closed-loop pole locations, presented in Figs. 7 and 8. The corresponding frequency and damping coefficient data are in Table 3. These data reveal that ASAC mainly affected the natural frequencies of the structure, whereas the greatest effect of vibration control was to increase the structural damping. This demonstrates the different mechanisms inherent to the acoustic and vibration control schemes, resulting from the different control design criteria.

Because of the aforementioned proximity of the second and third natural frequencies, the effect of second mode controllers on the location of the third mode poles merits particular attention. Figure 8 shows that the second mode vibration controller significantly increased the closed-loop damping of the third mode without affecting its natural frequency. From the viewpoint of acoustic control, this effect is undesirable because it increased the closed-loop radiation

Table 2 SPLs for open- and closed-loop systems

		Acoustic control		Vibration control	
Mode	Open-loop	SPL, dB	% reduction	SPL, dB	% reduction
1st	95	49	48	56	41
2nd	96	64	34	70	28

Table 3 Open- and closed-loop natural frequencies, Hz, and associated damping coefficients for acoustic and vibration control

	1st mode		2nd mode		3rd mode	
Control	Frequency	ζ	Frequency	ζ	Frequency	ζ
Open loop	216.02	0.0068	345.18	0.0108	363.52	0.0114
Acoustic, 1st mode	167.42	0.6573	236.24	0.0608	344.51	0.0344
Acoustic, 2nd mode	187.58	0.1329	318.32	0.0671	356.80	0.0144
Vibration, 1st mode	217.31	0.6399	275.54	0.2288	321.04	0.0719
Vibration, 2nd mode	206.21	0.2121	320.85	0.0666	363.52	0.3073

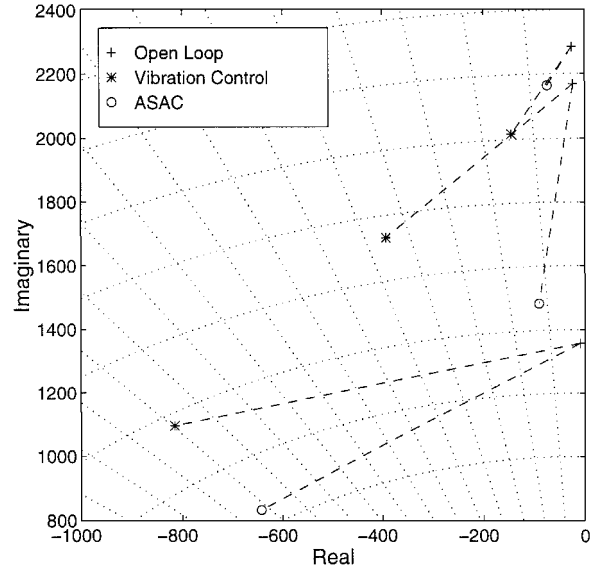

Fig. 7 Pole location map: first mode control.

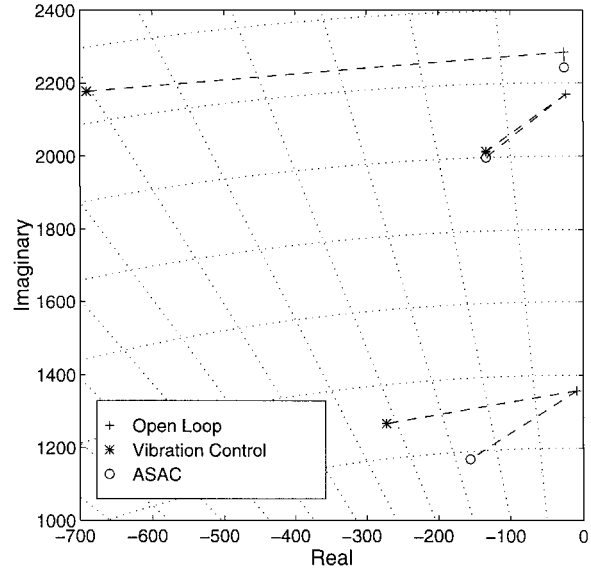

Fig. 8 Pole location map: second mode control.

efficiency of the third mode. The second mode acoustic controller, however, had very little effect on the third mode pole location, leaving its low radiation efficiency intact.

Additional understanding of the physical phenomena behind acoustic and vibration control can be gained by examining the shape of the structural velocity and the distribution of its wave number domain transformation, shown in Figs. 4 and 5, respectively, for the second structural mode. Both the acoustic and the vibration controllers were able to attenuate the structural velocities. ASAC resulted in a less regular closed-loop vibrational shape, usually leading to lower sound radiation power. The transformed velocity field shows that ASAC resulted in a slightly less radiating shape (smaller volume of the transformed velocity over the radiating circle) that accounts for its greater SPL reduction.

Conclusions

A methodology for the design of ASAC was presented. Acoustic structural and piezoelectric FE analysis was shown to provide a powerful tool for ASAC design. The structure dynamics model, which includes simple yet accurate model of piezoelectric actuation and sensing, is presented in state-space form. The acoustic power radiated by the vibrating structure into the far field is expressed as a quadratic form of the system states that is then used in the design of an $\mathcal{H}_\infty$ disturbance rejection controller. ASAC of a thin cylindrical panel was synthesized using this methodology. The superiority of the proposed control methodology over conventional vibration control was demonstrated. The ASAC controller proved less sensitive to variations in excitation frequency, outperforming the vibration controller in cases of undesirable spillover due to dense natural modes of flexible thin-walled cylinders.

Acknowledgment

The work reported in this paper is part of a Ph.D. Dissertation of the second author carried out at the Faculty of Aerospace Engineering, Technion—Israel Institute of Technology.

References

[1]Crawley, F., and de Luis, J., "Use of Piezoelectric Actuators as Elements of Intelligent Structures," *AIAA Journal*, Vol. 25, No. 10, 1987, pp. 1373–1385.

[2]Wang, B.-T., "Active Control of Far-Field Sound Radiation by a Beam with Piezoelectric Control Transducers: Physical System Analysis," *Smart Materials and Structures*, Vol. 3, No. 4, 1994, pp. 476–484.

[3]Pletner, B., and Abramovich, H., "A Consistent Methodology for the Modeling of Piezolaminated Shells," *AIAA Journal*, Vol. 35, No. 8, 1997, pp. 1316–1326.

[4]Clark, R., and Fuller, C., "Active Structural Acoustic Control with Adaptive Structures Including Wavenumber Considerations," *Journal of Intelligent Materials Systems and Structures*, Vol. 3, No. 2, April 1992, pp. 296–314.

[5]Mathur, G. P., and Tran, B. N., "Wavenumber Active Structural Acoustic Control for Smart Structures," *Proceedings of the AIAA 15th Aeroacoustics Conference*, AIAA, Washington, DC, AIAA Paper 93-4422, 1993.

[6]Clark, R., and Fuller, C., "Active Control of Structurally Radiated Sound from an Enclosed Finite Cylinder," *Journal of Intelligent Materials Systems and Structures*, Vol. 5, No. 3, May 1994, pp. 379–391.

[7]Mathur, G. P., and Tran, B. N., "Aircraft Cabin Noise Reduction Tests Using Active Structural Acoustic Control," *Proceedings of the AIAA 15th Aeroacoustics Conference*, AIAA, Washington, DC, AIAA Paper 93-4437, 1993.

[8]Gawronski, W., "Balanced Control of Flexible Structures," Springer–Verlag, Berlin, 1996, pp. 20–97.

[9]"ANSYS User's Manual," rev. 5.0, Swanson Analysis Systems, Houston, PA, 1992.

[10]Pletner, B., and Abramovich, H., "Actuation and Sensing in Piezolaminated Anisotropic Shells: Theoretical, Numerical and Experimental Investigation," TR TAE779, Technion—Israel Inst. of Technology, Haifa, Israel, May 1996.

[11]Pletner, B., "Active Control of Sound Radiated by Vibrating Thin-Walled Structural Elements," Ph.D. Dissertation, Faculty of Aerospace Engineering, Technion, Haifa, Israel, Dec. 1997.

[12]Bathe, K., *Finite Element Procedures in Engineering Analysis*, Prentice–Hall, Upper Saddle River, NJ, 1982, pp. 717–726.

[13]Cremer, L., and Heckl, M., *Structure-Borne Sound*, Springer–Verlag, Berlin, 1973, pp. 456–499.

[14]Maciejowski, J., *Multivariable Feedback Design*, Addison–Wesley, Longman, Reading, MA, 1989, pp. 265–324.

[15]Fuller, C., Elliot, S., and Nelson, P., *Active Control of Vibration*, Academic, New York, 1996, pp. 223–306.

[16]Turner, J., and Pretlove, A., *Acoustics for Engineers*, Macmillan, New York, 1991, pp. 14–17, 32–54.

[17]Balas, G., Doyle, J., Glover, K., Packard, A., and Smith, R., "μ-Analysis and Synthesis Toolbox (For Use with MATLAB)," MathWorks, Inc., and MUSYN, Inc., Natick, MA, 1995.